Journal of Asian Earth Sciences 114 (2015) 258–265

Contents lists available at ScienceDirect

Journal of Asian Earth Sciences

journal homepage: www.elsevier.com/locate/jseaes

Magnetostratigraphy and its paleoclimatic significance of the PL02 borehole in the Yinchuan Basin

Junping Wang [a,*], Miaomiao Shen [a], Jianmin Hu [b], Mingjian Wei [a], Xiaohong Zhao [a], Shaochang Liu [b], Xiaolei Li [a], Xinling Li [a]

[a] College of Resource Environment and Tourism, Capital Normal University, Beijing 100048, People's Republic of China
[b] Institute of Geomechanics, Chinese Academy of Geological Sciences, Beijing 100081, People's Republic of China

ARTICLE INFO

Article history:
Received 18 March 2015
Received in revised form 3 July 2015
Accepted 13 July 2015
Available online 13 July 2015

Keywords:
Magnetostratigraphy
Palaeoenvironment
Palaeomagnetic
Frequency-dependent susceptibility

ABSTRACT

The basin sediment provides an important means of studying regional tectonic actives; however, regional climate factors, overlaying tectonic actives, affect the sedimentary process in the basin. Because of the lack of long-term scales data, the research on climate change in the arid and semi-arid region is limited. The PL02 core, located in the center area of deposition in the Yinchuan Basin, has a thick deposit with a higher resolution and sedimentation rate, making itself practical for the reconstruction of the paleoclimate and the coupling relationship between regional tectonic activities and climate change.

The study of the 720-m borehole near Pingluo County is presented in this paper. The chronostratigraphic sequence of the core is established by palaeomagnetic dating. The magnetostratigraphic correlation to the geomagnetic polarity timescale shows that the PL02 core recorded the Brunhes, Matuyama, Gauss, Jaramillo, Olduvai, Kaena and Mammoth polarity chron or subchron. The sedimentation rate and the magnetostratigraphic of the core indicate that the onset of the PL02 core in this section occurred at ~3.4 Ma BP. The analysis of the core established a detailed chronological framework for regional geological research. At the stage of 3.22–3.04 Ma, 2.581–1.95 Ma and after 0.012 Ma, the sedimentation rate increases gradually, which archive three regional tectonic subsidence events.

The frequency-dependent susceptibility of the sediment is used to reconstruct the paleoclimatic change. The frequency-dependent susceptibility is more effective than the magnetic susceptibility on reflecting regional climate change in the basin. From 3.4 to 0.467 Ma, the gradual decrease of frequency-dependent susceptibility reflects the regional climate change from warm and humid to cold and dry. Since 0.467 Ma, the gradual increase of the frequency-dependent susceptibility corresponds to the climate becoming warm and humid again.

1. Introduction

The Yinchuan Basin is a Cenozoic fault basin. The Cenozoic evolution of the tectonic stress field of the basin is controlled by the interaction between the Ordos block in the east, the Alxa block in the west and the Tibetan Plateau block in the southwest. There are various types of faults in the basin and its peripheral mountains, which is controlled by different tectonic backgrounds and mechanisms (Zhang et al., 1998; Deng et al., 2003; Li and Li, 2008; Liu et al., 2010; Wang et al., 2011). The tectonic activity is intensive. The fault activity, the formation and the evolution of the basin have long been the focus of debate (Ma et al., 1982; Liu, 1998; Liu et al., 1990; Darby and Ritts, 2002; Hou et al., 2012; Huang et al., 2013; Cheng et al., 2014). In addition, the region lies in the transition zone of arid and semi-arid climates, which has recently become a focus of research of the East-Asian monsoon and global climate change.

The Yinchuan Basin continues to sink and receive the eroded materials from the surrounding mountains and plateaus, which causes thick sediments in the basin. The deposition of the continental sedimentary basin is generally regarded as an important component of the alluvial and fluvial archive, which provides reliable evidence for regional tectonic activity or long-timescale climatic fluctuation. Therefore, the sedimentary characteristics (such as sedimentary facies, chemical composition, grain size, susceptibility and so on) of the basin have become a popular topic for research (Zheng and Liu, 1994; Lin et al., 2001; Zhang et al., 2010a,b).

* Corresponding author.
E-mail address: jpwang@cnu.edu.cn (J. Wang).

http://dx.doi.org/10.1016/j.jseaes.2015.07.017
1367-9120/

Previous studies have performed many drillings to analyze the development and activity of faults in the case of bedrock (Research Group AFSOM, 1988; NBGMR, 1989). However, the sediment cores are usually short and only span part of the Quaternary period (Zheng and Liu, 1994; Tong et al., 1995, 1998). Although some sediment cores are long, the sampling density is too low to rebuild the sediment transport and deposition process in detail, and even worse, some of the cores have not been studied regarding dating (NBGMR, 1989). To some extent, the weak precision of the instrument also limits further research. In general, the results of the study are questionable (Research Group AFSOM, 1988; Zheng and Liu, 1994). This paper describes a detailed study of the magnetic stratigraphy of the Pingluo PL02 borehole in the Yinchuan Basin. Through establishing a chronological framework and analyzing the relationship between frequency-dependent susceptibility, magnetic susceptibility and the regional environmental change, this paper provides basic data for the regional tectonic activity.

2. Geological setting

The Yinchuan Basin, which is also known as the Yinchuan Graben, is located in the northeast of Tibetan Plateau; the area has experienced a multi-period intensive uplift and has a great effect on the landform evolution of the adjacent areas in Cenozoic (Molnar and Tapponnier, 1975; Zhang et al., 1990). The Yinchuan Basin is located to the east of Helan Mountain, which has an altitude of more than 3500 m, and to the west of the Ordos Plateau, which has an average altitude of approximately 1500 m, and it is covered by desert in the north and loess in the south.

The basin has a NNE–SSW trend. The Yinchuan Basin is 165 km in length from south to north, 42–60 km in width from east to west, and has an area of 7790 km^2. As a rifted basin, the Yinchuan Basin developed on the basis of the Yinchuan anticlinorium, which was formed by the intensive compression of the blocks in the Mesozoic (Darby and Ritts, 2002). The eastern and western boundaries of the basin are the Yellow river fault and the eastern margin fault of Helan Mountain, respectively. The southwestern boundary is the Niushoushan fault, and the northern boundary is the Zhengyiguan fault (NBGMR, 1989) (Fig. 1). The NNE trending faults in the basin are almost parallel to each other, which controls the NNE–SSW trend of the rifted basin. The basin is mainly filled by Cenozoic sediments, the thickness of which is more than 7500 m near the axis. Most of the bases of the tertiary sediments belong to the Paleozoic strata, and a few belong to the Cretaceous strata. The thickness of Quaternary sediment alone is up to 2000 m by the speculation of geophysical prospecting (NBGMR, 1989). The current measurements at the Earth's surface show that the Yinchuan Basin is still in intermittent subsidence. The sediment rate of the basin is 0.22 cm per year, on average, relative to Helan Mountain (NBGMR, 1989). The Yellow River, which originates in the Tibetan Plateau, runs through the basin from south to north and carries a large amount of mud and sand into the basin.

With a temperate continental climate, the Yinchuan Basin is dry and cold in winter, which is dominated by prevailing north winds, but is always sunny in summer. The annual average temperature is 5.7–9.5 °C and decreases gradually from the north to the south. The annual temperature range is large. Affected by monsoon, the annual average precipitation is 170–200 mm, with a gradual reduction from south to north. Usually, precipitation is concentrated in summer; in particular, the precipitation in July and August accounts for more than 50% of annual precipitation. The annual average evaporation is 1829.1 mm (NBGMR, 1989). The land cover between east and west of the basin is different: it is semi-arid grassland vegetation in the east, while it has an arid desert landscape in the west.

From west to east, the main topography units of the study region are the middle relief mountain (Helan Mountain), piedmont pluvial floodplain (composed of many pluvial fans), and alluvial floodplain (the Yellow River valley).

3. Materials and methods

This paper mainly discusses the magnetostratigraphy of the Yinchuan Basin and its paleoclimatic significance based on the records of a drilling core. The location of sampling drilling is 38° 55′26.62″N, 106°36′3.82′E, with an altitude of approximately 1103 m. The location is approximately 11 km west of the Yellow River and 22 km east of Helan Mountain. The sampling drilling is performed on the east side of Yinchuan-Pingluo fault and on the alluvial floodplain. The length of drilling core is 720 m.

The model of the drilling rig is XY-6B with a hydraulic impact-rotary system, which was made in China. A triple tube swivel type rotary corer is applied in the drilling. In the process of drilling, the core samples are directly packed into the polyvinyl chloride tube that is the inner-most tube of the triple drilling pipe, which reduces the external disturbances for the sediment core. The wall of the core has been consolidated with casing pipes from 0 to 70 m and mud protection from 70 to 720 m in depth. The drilling work took over two months and was completed in August, 2013.

The great thickness of the Quaternary deposit is consistent with the sedimentation rate of the Yinchuan Basin, which provides a convenient means for core dating. We collected magnetic stratigraphy samples of the drilling to obtain a more precise age. Generally, the oriented block samples are collected at 0.2-m intervals. Depending on the core recovery rate of the sediments (the core recovery rate is 94.7%), small amounts of the sampling intervals are as large as 0.4–1.0 m. Each sample was processed indoors according to the lithological characteristics. Each clayey core sample is cut into three sets of cube specimens, each with a size of $2 \times 2 \times 2$ cm^3. Each sandy core sample is made into cylinders and placed into three glass tubes with a size of 2 cm in height and 2 cm in diameter, which are sealed by silicone. A total of 3400 directional samples are obtained. The paleomagnetic measurements are performed on a 2G-755R Superconducting Rock Magnetometer in the paleomagnetic and rock magnetism laboratory, Institute of Earth Environment, Chinese Academy of Sciences. The measured specimens include 1837 thermal demagnetization specimens and 747 alternating demagnetization specimens. The processing and measurement of all of the specimens are performed in a magnetically shielded environment. Thermal demagnetization specimens are heated by the TD-48 Thermal Demagnetizer and then measured using a 2G-755 Superconducting device. A system thermal demagnetization mode is adopted with 16 steps, which are at 25 (at room temperature), 100, 120, 150, 200, 250, 300, 350, 400, 450, 500, 550, 580, 600, 650 and 675 °C. The alternating demagnetization specimens are directly measured using a 2G-755 Superconducting device. The measurements are performed in 15 steps: 0, 50, 80, 100, 120, 150, 200, 250, 300, 350, 400, 450, 500, 600, 700 and 800 Gauss for system demagnetization.

To obtain the top age of the core, eight ^{14}C samples are taken in the upper part of the core, where the organic matter is relatively rich and the sediment which is dark in color, varies from blue gray to black. All samples were submitted to Beta Analytic Inc. for AMS radiocarbon dating. Radiocarbon ages were calibrated by the INTCAL13 calibration curve (Reimer et al., 2013) and are showed as 2 sigma standard deviation and mean calibration ages (Table 1).

The powder samples are taken at 0.1-m intervals from the core for magnetic susceptibility measurements. A total of 6692 samples are collected. These samples are air-dried in the laboratory and

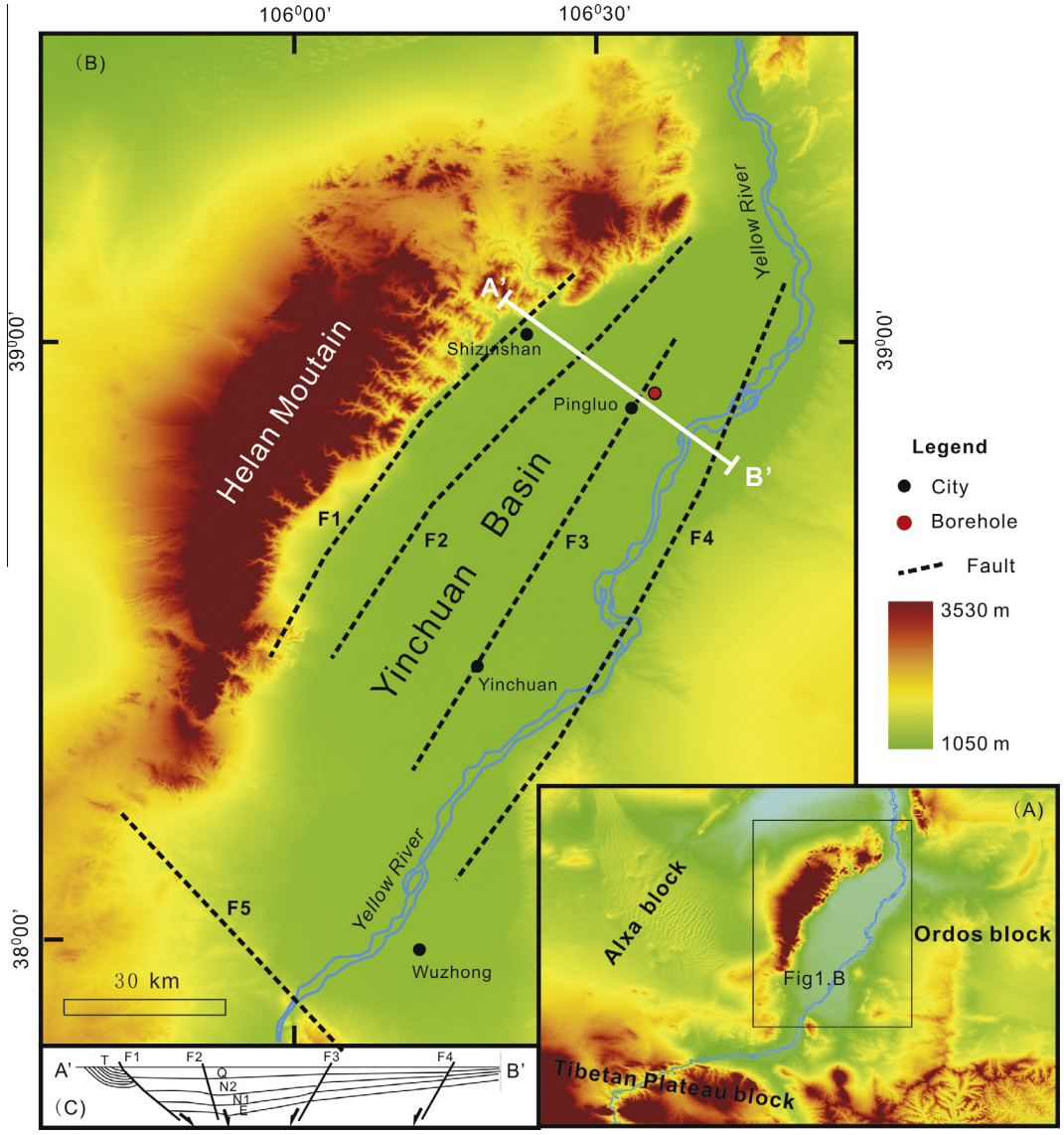

Fig. 1. Sketch of the study region. (A) A digital elevation model (DEM) image showing the Yinchuan Basin distribution. The black rectangle outlines the region of the Yinchuan Basin. (B) Main faults in the basin. F1: Easter margin fault of Helan Mountain; F2: Luhuatai fault; F3: Yinchuan-Pingluo fault; F4: Yellow River fault; F5: Niushoushan fault. (C) Geologic cross-section (A′–B′) from Helan Mountain in the west to the Yellow River in the east, as shown in (B).

then gently grinded and measured using a Bartington MS2 magnetic susceptibility meter to obtain the magnetic susceptibility.

4. Results and discussion

4.1. Paleomagnetism and dating

The results of thermal demagnetization (Fig. 2) show that the remanent magnetization of the majority of specimens contains two parts: a low temperature component and a high temperature component. At low temperature, the remanence and its direction change is relative large. A turning point appears when the demagnetization temperature increases to 250 °C or 300 °C. With the continuously rising temperature, the trajectory of the vector is relatively stable, the end point is toward the origin, and the remanent magnetization gradually decreases (high temperature component), which shows that the secondary remanent magnetization is cleaned out and that the native characteristic remanent magnetization is obtained. However, there are still some individual samples for which the secondary viscous remanent magnetism and isothermal remanent magnetization of the specimens are not cleaned until the demagnetization temperature reaches 500 °C or 580 °C.

Under the condition of alternating demagnetization, the trajectory of demagnetization changes at 100 and 500 Gauss, with a decrease of the remanent magnetization; subsequently, the primary remanent magnetization is obtained (Fig 2). There are only a few specimens that have a secondary remanent magnetism that cannot be cleaned; these specimens can be cleaned by thermal demagnetization. The results show that the magnetic characteristics are various. Goethite is the main magnetic mineral, and greigite or pyrrhotite may be included. In addition, maghemite and magnetite occupy a certain proportion. The measurement results of the characteristic remanent magnetization of the thermal demagnetization are shown in Fig. 3. The characteristics of alternating demagnetization and the changes of thermal demagnetization are similar. The directions of the characteristic remanent magnetization (ChRM) are calculated using the least-squares fitting technique (Kirschvink, 1980).

Table 1
Radiocarbon ages in years BP and calibrated of the Pingluo core.

Code. lab	Depth (m)	Conventional radiocarbon age (yr BP)	2 Sigma calibrated radiocarbon age (cal yr BP) (95% probability)	Mean calibrated radiocarbon age (cal yr BP)
Beta-394162	2.8	3490 ± 30	3840–3690	3655
		3660–3650		
Beta-399959	8.0	7680 ± 30	8540–8410	8425
Beta-402814	8.2	7500 ± 30	8380–8300	8340
		8255–8215		
Beta-399960	8.8	6820 ± 30	7690–7610	7650
Beta-402815	13.0	7170 ± 30	8020–7950	7985
Beta-394163	13.2	29,580 ± 150	33,960–33,565	33762.5
Beta-399961	14.8	7860 ± 30	8715–8590	8652.5
Beta-399962	16.8	12,930 ± 40	15,600–15,295	15447.5

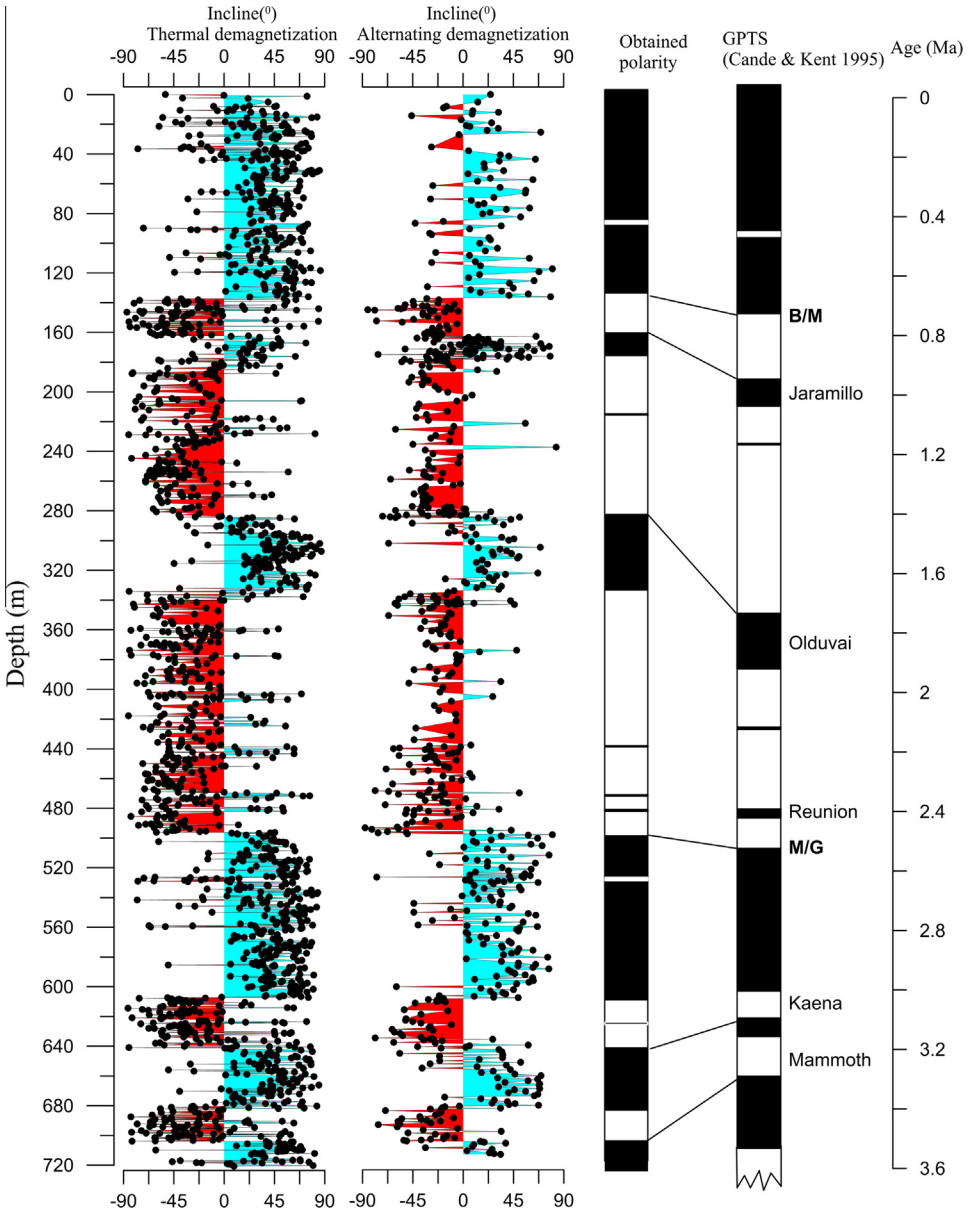

Fig. 2. Result of the thermal demagnetization and alternating demagnetization of the PL02 core and their correlations with the geomagnetic timescale.

The remnant magnetization is mainly of normal polarity at the layer of 0–137.2 m and of reversed polarity at 137.2–496.3 m in depth, with two instances of normal polarity at 162.4–179 m and 284.3–333.8 m. Subsequently, the remnant magnetization returns to normal polarity at 496.3–720 m, with two layers of reversed polarity at 606.8–640.3 m and 680.3–704.1 m (Fig. 3).

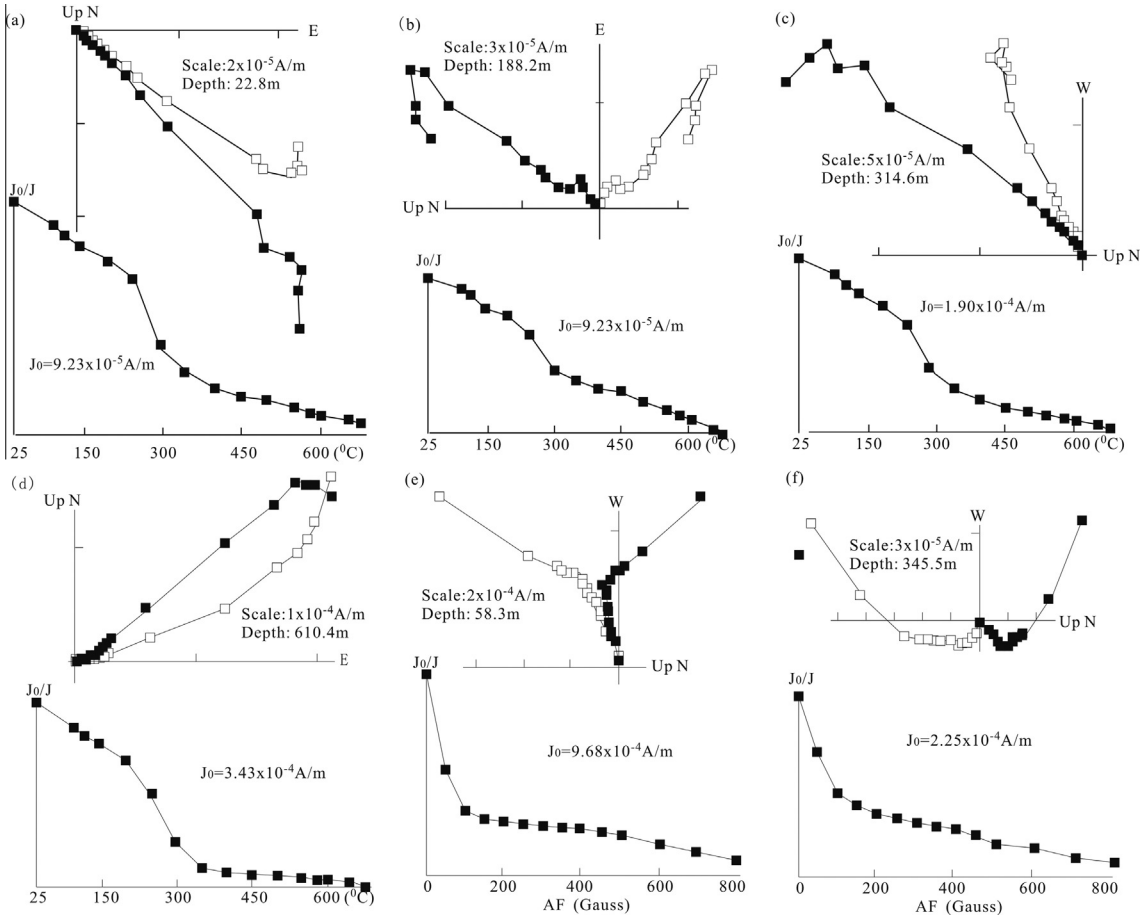

Fig. 3. Representative demagnetization diagrams of both thermal (a–d) and alternating demagnetization (e–f). Solid (hollow) square plot inclination (declination) within the orthogonal demagnetization diagrams; NRM denotes the natural remnant magnetization.

Compared with the geomagnetic polarity timescale (GPTS) (Cande and Kent, 1995), the layer of 0–137.2 m is the Brunhes normal chron, 137.2–496.3 m is the Matuyama reversed chron and 496.3–720 m is the Gauss normal chron. Among them, the layers of 162.4–179.0 m and 284.3–333.8 m are the Jaramillo and Olduvai normal subchron, respectively. Those at 606.8–640.3 m and 680.3–704.1 m are the Kaena and Mammoth reversed subchron, respectively. The main polarity and sub-polarity periods of alternating demagnetization are consistent with those of the thermal demagnetization, which further confirms the reliability of the thermal demagnetization.

The normal polarity without reversal polarity at the bottom of the core indicates that the bottom is still in the Gauss normal chron. The age of 680.3–704.1 m, which corresponds to the Mammoth reversed subchron, spans from 3.33 to 3.22 Ma, with the sedimentation rate circa 0.216 m/kyr. By this calculation, the age of the core bottom is approximately 3.4 Ma.The top 0.83 m-thick deposition of the borehole was disturbed and deposited by human activities. To develop a reliable chronological framework, 8 radiocarbon samples were measured. The result (Table 1) is mostly consistent with the age–depth model except the lab No Beta-394163 which may be older because of leaching and moving of the groundwater. Based on the other 7 radiocarbon calibrated ages (Table 1, mean calibrated age), a line trend equation has been deduced:

$$y = 598.2x + 2405 \quad (R^2 = 0.679)$$

where y is the derived age (cal yr BP), and x is the depth (m) of the core.

Using the derived linear equation, you can then obtain that the ages at the depth of 2.8 m and 16.8 m are 4080 cal yr BP and 12,455 cal yr BP (circa 0.012 Ma) respectively.

Combined with other polar reversal boundary age (Table 2), the age-depth curve is close to a straight line (Fig. 4), which indicates that a reasonable calculation was performed. Therefore, the deposition of the borehole started at circa 3.4 Ma BP. The age within the interval between polarity reversal boundaries (or the ^{14}C age) can

Table 2
Boundary age and sedimentation rate of the core in Pingluo.

Depth of Borehole/m	Boundary type	Age/Ma BP	Sedimentation rate/m/kyr
0.83	[a]	0	
2.8	Derived from 14C	0.004080	0.483
16.8	Derived from 14C	0.012455	1.672
137.2	B/M	0.78	0.166
162.4	Top of Jaramillo	0.99	0.120
179	Bottom of Jaramillo	1.07	0.208
284.3	Top of Olduvai	1.77	0.150
333.8	Bottom of Olduvai	1.95	0.275
496.3	M/G	2.581	0.258
606.8	Top of Kaena	3.04	0.241
640.3	Bottom of Kaena	3.11	0.479
680.3	Top of Mammoth	3.22	0.364
704.1	Bottom of Mammoth	3.33	0.216
720.7	[b]	3.40	0.216

[a] The top 0.83 m-thickness deposition is disturbed and deposited by human activities.
[b] Calculated by sedimentation rate of Mammoth subchron.

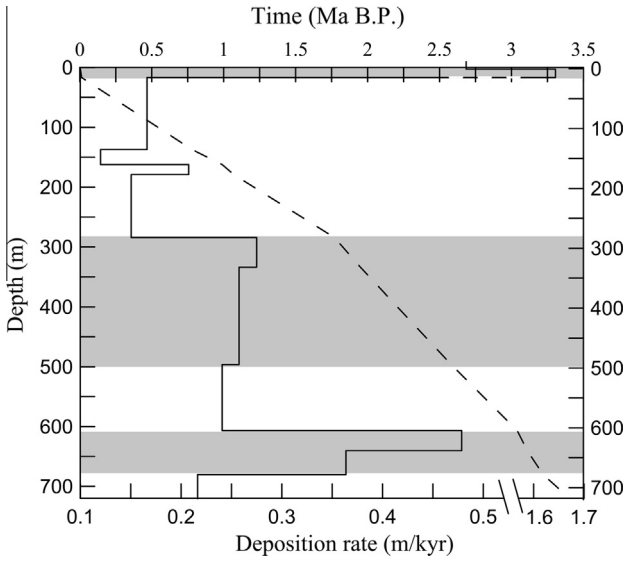

Fig. 4. Variation of the depth-age (dotted line) and sedimentation rates (solid line) of the PL02 core.

be calculated by a linear interpolation between adjacent magnetostratigraphic control points.

4.2. Sedimentation rate and tectonic activities

The sedimentation rates are quite different at various periods, which can be divided into four stages (Fig. 4). From 3.4 to 3.04 Ma, the sedimentation rate increases gradually, which is high in the whole core and is up to 0.478 m/kyr at the end of the stage. At 3.04–1.77 Ma, the sedimentation rate increases gradually and is up to 0.275 m/kyr, which is slightly lower than that at the previous stage. At 1.77–0.012 Ma, the sedimentation rate is the lowest in the whole core. After 0.012 Ma (or during the Holocene), the sedimentation rate increases rapidly.

The sedimentation rate of the basin is mainly related to the regional tectonic activity and climate change. The tectonic activity mainly caused the periodic change of the sedimentation rate in this area. The borehole is located in the central of the flat Yinchuan Basin and is far from the mountains. The borehole is approximately 22 km east of Helan Mountain and more than 135 km north of the southern mountains (Fig. 1). When the Yellow River flows from southern mountains (which lie on the Tibetan Plateau block) into the Yinchuan Basin, the carrying capacity of the river decreases, which is a response to the rapidly decreasing channel gradient. Subsequently, the river flows from southwest to northeast in the basin and runs through Pingluo. Thus, the particle size of the sediment near Pingluo is fine, composed mainly of medium sand, fine sand, and clay (Fig. 5). The sediments of the core also mainly consist of medium sand, fine sand and clay. The effect of climate change on the sedimentation rate in the central basin is quite small relative to the edge of the basin. In addition, the sedimentation rates of the core are high, except the third stage. For the center of the basin, the highest sedimentation rate is 1.672 m/kyr, which may not be dominated by climate.

From the viewpoint of fluvial landscape evolution, the timing of the river incision is dominated by climate change in the context of tectonic activity (Pan et al., 2009). The frequency of climate change is higher than that of tectonic activity. As a result, tectonic activities can often be recorded by river incision and erosion materials depositing rapidly in a low-lying basin. The sedimentation rates of the core increase rapidly at the stage of 3.22–3.04 Ma, 2.581–1.95 Ma and after 0.012 Ma. In particular, the sedimentation rate of the core has changed dramatically and reached a high value since 0.012 Ma. This result shows that three tectonic activities may have occurred along with a relative subsidence and a high sedimentation rate since 3.4 Ma in this area.

4.3. Frequency-dependent susceptibility

Low-frequency mass magnetic susceptibility (also known as magnetic susceptibility) and frequency-dependent susceptibility are important indicators for the climate research. In the loess-paleosol profiles, the magnetic susceptibility of paleosol is of high value, while that of loess is of low value. The paleosol layer corresponds to the warm interglacial climate and has strong pedogenesis, which causes the frequency-dependent susceptibility to have a high value. The loess layer corresponds to a cold glacial climate that makes the frequency-dependent susceptibility have a low value (Liu, 1985; Kukla et al., 1988; Maher and Thompson, 1991). However, for fluvial sediment, the climate characteristics indicated by the value of magnetic susceptibility are much more complicated. Many factors, such as the terrain, water power, water depth of sediment and land cover, are likely to lead to a change of magnetic susceptibility (Thompson and Oldfield, 1986; Dunlop and Ozdemir, 1997; Wang et al., 2008; Xu et al., 2010; Gerald et al., 2015). The indicating significance shown by magnetic susceptibility may be different in different regions; sometimes it is even opposite for the different response modes to climate and environment (Hagen and Nicolas, 1999; Zhang et al., 2010b).

Frequency-dependent susceptibility reflects features of superparamagnetic ferromagnetic minerals with very fine particles (smaller than 0.035 μm) or viscous ferromagnetic minerals for which the particle size is nearly stable at the single-domain boundaries. These minerals are one of major contributors to the magnetic susceptibility of deposits formed by weathering and pedogenesis (bacteria or chemical processes in the soil) (Thompson and Oldfield, 1986; Oldfield, 1991). The climatological significance revealed by frequency-dependent susceptibility is more direct than that revealed by magnetic susceptibility in this core (Fig. 5).

The frequency-dependent susceptibility of the Pingluo core exhibits some obvious change in the stages (Fig. 5A), though the value of the frequency-dependent susceptibility is very low. At the stage of 3.4–2.41 Ma, the frequency-dependent susceptibility value is high and fluctuates with a large amplitude. At 2.41–1.84 Ma, the value and fluctuation of the frequency-dependent susceptibility is lower than that at the previous stage. At 1.84–0.467 Ma, the value and fluctuation of the frequency-dependent susceptibility is the lowest; since 0.467 Ma, it increased again. In summary, the frequency-dependent susceptibility decreased gradually and periodically from 3.4 Ma to 0.467 Ma. Conversely, the magnetic susceptibility slowly increased at this time (Fig. 5B).

The study area is located in the arid and semi-arid transition zone. In warm and humid periods, the chemical weathering, biological process and pedogenesis are strong, which causes the formation of fine particle minerals (such as superparamagnetic, stable single domain and multi-domain grain). Although most of the superparamagnetic may be dissolved in a reducing condition (Anderson and Rippey, 1988; Snowball, 1993; Evans et al., 1997; Hagen and Nicolas, 1999) during the humid climate period, a very small amount of superparamagnetic grains remain preserved in the sediment since many superparamagnetic grains have developed in warm-humid climatic conditions, which is the contributor of the frequency-dependent susceptibility. Thus, the frequency-dependent susceptibility is relatively high with a large fluctuation at the first stage in the core. Conversely, in the cold and dry period, with less precipitation, the physical weathering is strong, but the chemical weathering and pedogenesis is weak,

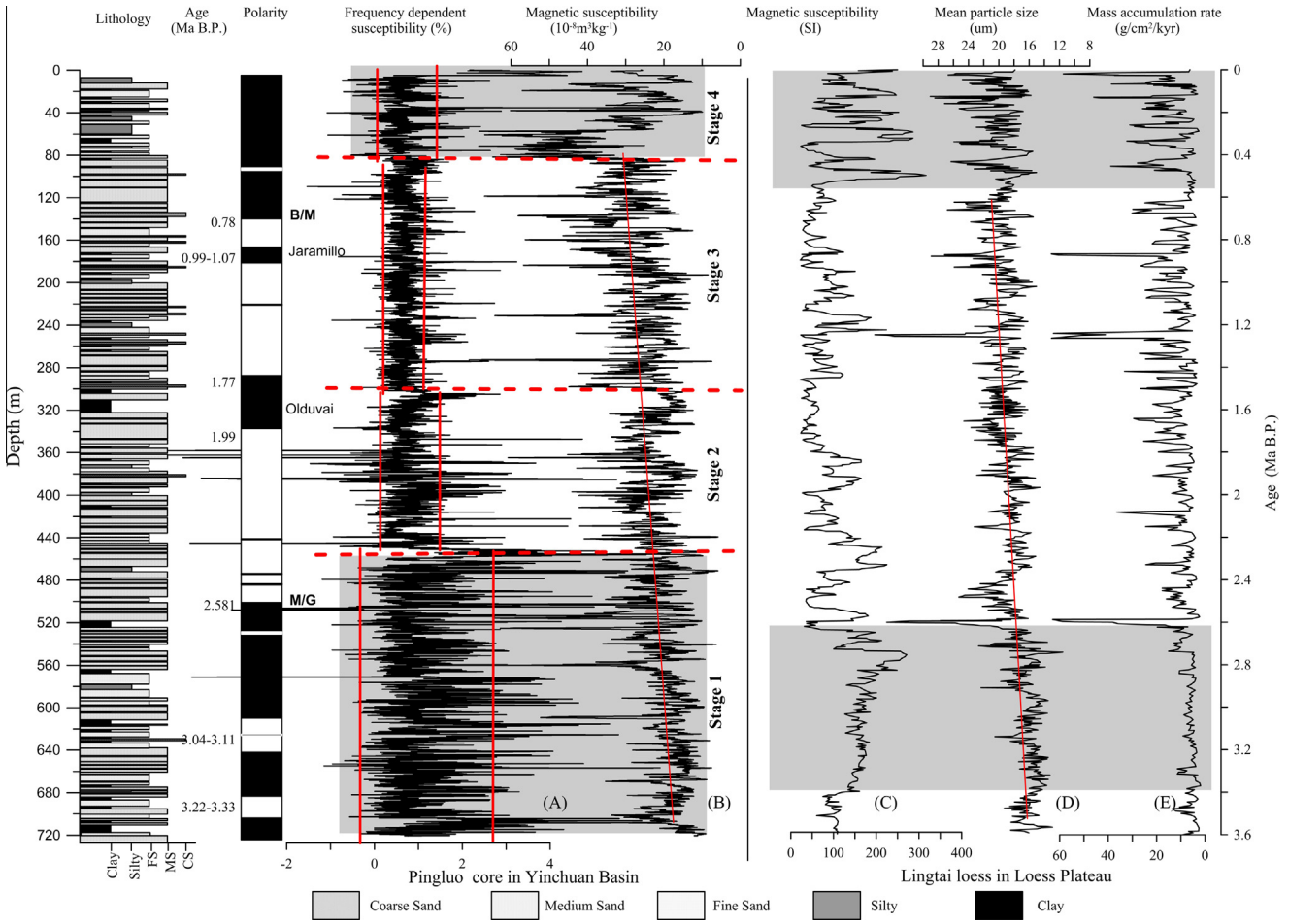

Fig. 5. Lithostratigraphy and magnetostratigraphy of the PL02 core and its variation curves compared to Lingtai loess record (Sun and An, 2005). (A) frequency-dependent susceptibility and (B) magnetic susceptibility of Pingluo core. (C) Magnetic susceptibility, (D) mean particle size and (E) mass accumulation rate of Lingtai loess.

resulting in the frequency-dependent susceptibility having a low value with a small fluctuation. From 3.4 to 0.467 Ma, the gradual decrease of the frequency-dependent susceptibility indicates that the regional climate changed from warm and humid to cold and dry. Since 0.467 Ma, the gradual increase of the frequency-dependent susceptibility indicates that the climate became warm and humid again.

The trend of the magnetic susceptibility and the trend of the frequency-dependent susceptibility are opposite in value. From 3.4 to 0.467 Ma, the magnetic susceptibility increased gradually, but it began to decrease since 0.467 Ma. In warm and humid periods, with high precipitation and a high groundwater level, the sediment is in a super reducing condition fluvio-lacustrine environment and the magnetic susceptibility is low. In the cold and dry period, with less precipitation and low groundwater level, the oxidation is strong with high magnetic susceptibility, which is consistent with the climatic tendency that changed from warm and humid to cold and dry according to the frequency-dependent susceptibility.

The climatic temporal changes recorded by the loess in Lingtai (Sun and An, 2005) and other sections (Nie et al., 2014) exhibit some similar trends with those of the sediment at Pingluo core, though the loess is considered to be a kind of eolian deposit which is different from the alluvial and fluvial deposit in Pingluo. The changes of the Lingtai loess section can be basically divided into three stages from the curves (Fig. 5C and D). In the first period (circa from 3.6 to 2.6 Ma), both the value and amplitude of the mass accumulation rate and the mean particle size are the lowest in the section (Fig. 5D and E). The magnetic susceptibility is high but has a small fluctuation (Fig. 5C). In the third period (circa from 0.55 Ma to present), both the value and amplitude of the magnetic susceptibility, mass accumulation rate and the mean particle size are high. The variations of the second period fall somewhere in between.

More important than all of those, the reconstructed mass accumulation rate demonstrates that the distinct aridity–humidity fluctuations occurred over glacial–interglacial timescales, and these were superimposed on a gradual long-term drying trend over the past 3.6 Ma (Sun and An, 2005). This drying trend is consistent with the archive of the Pingluo core, though there are still some differences which are under the control of the variations of the sedimentary environments and regional tectonic activities. More studies are needed to test this issue.

5. Conclusions

The paleomagnetic result of the Pingluo core revealed the detailed changes of the magnetic polarity reversals since 3.4 Ma because the borehole is up to 720 m and has a high sedimentation rate. The Brunhes, Matuyama, Gauss, Jaramillo, Olduvai, Kaena and Mammoth polarity chrons or subchrons are recorded as an archive. The results establish a detailed chronological framework for regional geological studies. At the stages of 3.22–3.04 Ma and 2.581–1.95 Ma and after 0.012 Ma, the sedimentation rate increases gradually, which archives three regional tectonic subsidence events.

Because Pingluo is located in an arid and semi-arid transition zone, the frequency-dependent susceptibility is more effective than the magnetic susceptibility in reflecting regional climate change. From 3.4 to 0.467 Ma, the gradual decrease of the frequency-dependent susceptibility reflects the regional climate change from warm and humid to cold and dry, even though the value of the frequency-dependent susceptibility was very low. Since 0.467 Ma, the gradual increase of the frequency-dependent magnetic susceptibility indicates that the climate became warm and humid again. The change of the magnetic susceptibility is relatively complex and requires further research.

Acknowledgements

We are grateful to the anonymous reviewers who examined the submitted manuscript and Qiang Xiaoke for experimental guidance. This research is financially supported by the Geological Investigation Project of China Geological Survey (1212011120099 and 1212011220259), the Beijing Natural Science Foundation (Grant No. 8132021) and the National Natural Science Foundation of China (Grant Nos. 41371210 and 41471007).

References

Anderson, N.J., Rippey, B., 1988. Diagenesis of magnetic minerals in the recent sediments of a eutrophic lake. Limnol. Oceanogr. 33, 1476–1492.

Cande, S.C., Kent, D.V., 1995. Revised calibration of the geomagnetic polarity timescale for the Late Cretaceous and Cenozoic. J. Geophys. Res. 100, 6093–6095.

Cheng, B., Cheng, S., Zhang, G., Zhao, D., 2014. Seismic structure of the Helan Liupan Ordos western margin tectonic belt in North-Central China and its geodynamic implications. J. Asian Earth Sci. 87, 141–156.

Darby, Brian J., Ritts, Bradley D., 2002. Mesozoic contractional deformation in the middle of the Asian tectonic collage: the intraplate Western Ordos fold-thrust belt, China. Earth Planet. Sci. Lett. 205, 13–24.

Deng, Q., Zhang, P., Ran, Y., Yang, X., Min, W., Chu, Q., 2003. Basic characteristics of active tectonics of China. Sci. China (Ser. D) 46, 356–373.

Dunlop, D.J., Ozdemir, O., 1997. Rock Magnetism: Fundamentals and Frontiers. Cambridge University Press, Cambridge, pp. 1–577.

Evans, M.E., Heller, F., Bloemendal, J., Thouveny, N., 1997. Natural magnetic archives of past global change. Surv. Geophys. 8, 183–196.

Gerald, T., Satria, B., John, K., James, R., Umar, F., Khoiril, M., Nurul, A., La, O.S., 2015. Variation of magnetic properties in sediments from Lake Towuti, Indonesia, and its paleoclimatic significance. Palaeogeogr. Palaeoclimatol. Palaeoecol. 420, 163–172.

Hagen, S., Nicolas, T., 1999. Rock-magnetic properties of Eemian maar lake sediments from Massif Central, France: a climatic signature? Earth Planet. Sci. Lett. 173 (3), 299–313.

Hou, X., Cui, H., Huan, Y., 2012. Analysis of structural style and tectonic evolution in Yinchuan Basin. J. Northeast Petrol. Univ. 36 (6), 28–33 (in Chinese with English abstract).

Huang, X., Shi, W., Li, H., Chen, L., Cen, M., 2013. Cenozoic tectonic evolution of the Yinchuang Basin: constraints from the deformation of its boundary faults. Earth Sci. Front. 20 (4), 199–210 (in Chinese with English abstract).

Kirschvink, J.L., 1980. The least-squares line and plane and the analysis of palaeomagnetic data. Geophys. J. Int. 62, 699–718.

Kukla, G., Heller, F., Liu, M., Xu, C., Liu, S., An, S., 1988. Pleistocene climates in China dated by magnetic susceptibility. Geology 16, 811–814.

Li, R., Li, Y., 2008. Tectonic evolution of the western margin of the Ordos Basin Central China. Russ. Geol. Geophys. 49, 23–27.

Lin, A.M., Yang, Z.Y., Sun, Z.M., Yang, T.S., 2001. How and when did the Yellow River develop its square bend? Geology 29, 951–954.

Liu, T., 1985. Loess and the Environment. China Ocean Press, Beijing, pp. 30–200.

Liu, S., 1998. The coupling mechanism of basin and orogen in the western Ordos basin and adjacent regions of China. J. Asian Earth Sci. 16, 369–383.

Liu, H., Lu, W., Wang, Y., 1990. Formation and deformation of fold-thrust belts in the western margin of Ordos block. In: Yang, J. (Ed.), Petroleum and Structure of the Western Margin of Ordos Basin. Gansu Science and Technology Publishing House, pp. 54–76 (in Chinese with English abstract).

Liu, J.H., Zhang, P.Z., Zheng, D.W., Wan, J.L., Wang, W.T., Du, P., Lei, Q.Y., 2010. Pattern and timing of late Cenozoic rapid exhumation and uplift of the Helan Mountain, China. Sci. China Earth Sci. http://dx.doi.org/10.1007/s11430-010-0016-0.

Ma, X., Deng, Q., Wang, Y., Liu, H., 1982. Cenozoic graben systems in North China. Z. Geomorphol. 42, 99–116, N.F. Berlin, Suppl-bd.

Maher, B.A., Thompson, R., 1991. Mineral magnetic record of the Chinese loess and paleosols. Geology 19, 3–6.

Molnar, P., Tapponnier, P., 1975. Cenozoic tectonics of Asia, effects of a continental collision. Science 189, 419–426.

NBGMR, 1989. Ningxia Bureau of Geology and Mineral Resources (NBGMR). Regional Geology of Ningxia Hui Autonomous Region. Geological Publishing House, Beijing, pp. 0–196 (in Chinese with English abstract).

Nie, Junsheng, Stevens, Thomas, Song, Yougui, King, John W., Zhang, Rui, Ji, Shunchuan, Gong, Lisha, Cares, Danielle, 2014. Pacific freshening drives Pliocene cooling and Asian monsoon intensification. Sci. Rep. 4, 5474. http://dx.doi.org/10.1038/srep05474.

Oldfield, F., 1991. Environmental magnetism – a personal perspective. Quat. Sci. Rev. 10, 73–85.

Pan, B., Su, H., Hu, Z., Hu, X., Gao, H., Li, J., Kirby, E., 2009. Evaluating the role of climate and tectonics during non-steady incision of the Yellow River: evidence from a 1.24 Ma terrace record near Lanzhou, China. Quat. Sci. Rev. 28, 3281–3290.

Reimer, Paula J., Bard, Edouard, Bayliss, Alex, Beck, J. Warren, Blackwell, Paul G., Bronk Ramsey, Christopher, Buck, Caitlin E., Cheng, Hai, Edwards, R. Lawrence, Friedrich, Michael, Grootes, Pieter M., Guilderson, Thomas P., Haflidason, Haflidi, Hajdas, Irka, Hatté, Christine, Heaton, Timothy J., Hoffmann, Dirk L., Hogg, Alan G., Hughen, Konrad A., Kaiser, K. Felix, Kromer, Bernd, Manning, Sturt W., Niu, Mu, Reimer, Ron W., Richards, David A., Scott, E. Marian, Southon, John R., Staff, Richard A., Turney, Christian S.M., van der Plicht, Johannes, 2013. IntCal13 and Marine13 radiocarbon age calibration curves 0–50,000 years cal BP. Radiocarbon 55 (4), 869–1887.

Research Group on Active Fault System around Ordos Massif (Research Group AFSOM), 1988. Active Fault System around Ordos Massif. Seismological Press, Beijing, pp. 1–142 (in Chinese with English abstract).

Snowball, I.F., 1993. Mineral magnetic properties of Holocene lake sediments and soils from the Karsa valley, Lappland, Sweden, and their relevance to palaeoenvironmental reconstruction. J. Quat. Sci. 5, 258–270.

Sun, Y., An, Z., 2005. Late Pliocene–Pleistocene changes in mass accumulation rates of eolian deposits on the central Chinese Loess Plateau. J. Geophys. Res. 110, D23101. http://dx.doi.org/10.1029/2005JD006064.

Thompson, R., Oldfield, F., 1986. Environmental Magnetism. George Allen & Unwin, London, pp. 1–104.

Tong, G.B., Shi, Y., Fan, S.X., Zhang, J.P., Song, X.H., Liu, Z.X., Qiao, G.D., Zhang, J.X., Zhang, M.Y., 1995. Environment features of Yinchuan basin in late Quaternary period. Earth Sci. – J. China Univ. Geosci. 20 (4), 421–425 (in Chinese with English abstract).

Tong, G., Shi, Y., Zheng, H., Zhang, J., Lin, F., He, Q., Song, X., Liu, Z., Qiao, G., Zhang, J., Yang, X., Zhang, W., 1998. Quaternary stratigraphy in Yinchuan Basin. J. Stratigr. 22 (1), 42–51 (in Chinese with English abstract).

Wang, X., Wu, L., Zhang, G., Wang, G., Han, W., 2008. Characteristics and environmental significance of magnetic susceptibility and grain size of lake sediments since Holocene in Chaohu Lake, Anhui Province. Sci. Geogr. Sin. 28 (4), 548–553 (in Chinese with English abstract).

Wang, Wei-tao, Zhang, Pei-Zhen, Eric, K., Wang, Li-Hua, Zhang, Guang-Liang, Zheng, De-Wen, Chai, Chi-Zhang, 2011. A revised chronology for Tertiary sedimentation in the Sikouzi basin: implications for the tectonic evolution of the northeastern corner of the Tibetan Plateau. Tectonophysics 505, 100–114.

Xu, X., Qiang, X., An, Z., Li, X., Li, P., Sun, Y., 2010. Magnetic susceptibility of Heqing drill core and its palaeoenvironmental implications. J. Geomech. 16 (4), 372–382 (in Chinese with English abstract).

Zhang, P., Burchfiel, B.C., Molnar, P., Zhang, W., Jiao, D., Deng, Q., Wang, Y., Leigh, R., Song, F., 1990. Late Cenozoic tectonic evolution of the Ningxia-Hui Autonomous Region, China. Geol. Soc. Am. Bull. 102, 1484–1498.

Zhang, Y., Mercier, J., Vergely, P., 1998. Extension in the graben systems around the Ordos (China), and its contribution to the extrusion tectonics of south China with respect to Gobi-Mongolia. Tectonophysics 285, 41–75.

Zhang, J., Dickson, C., Cheng, H., 2010a. Sedimentary characteristics of Cenozoic strata in central-southern Ningxia, NW China: implications for the evolution of the NE Qinghai-Tibetan Plateau. J. Asian Earth Sci. 39, 740–759.

Zhang, J., Yang, T., Li, Y., Zhang, S., 2010b. Analysis on the magnetic susceptibility and its influence factors of the lake sediments in the CH0310 Core of Qarhan, Paleolake, Qaidam Basin. Acta Sedimentol. Sin. 28 (4), 790–797 (in Chinese with English abstract).

Zheng, H.R., Liu, P.G., 1994. Research on Quaternary magnetostratigraphy and its geological significance in Yinchuan basin. In: Proceeding of the 10th Academic Congress of the Geophysical Society of China, pp. 349–350 (in Chinese).